Deficits in dopaminergic transmission precede neuron loss and dysfunction in a new Parkinson model

Stephanie Janezic[a,b,1], Sarah Threlfell[a,b,1], Paul D. Dodson[a,c,1], Megan J. Dowie[a,c], Tonya N. Taylor[a,b], Dawid Potgieter[a,b], Laura Parkkinen[a,d], Steven L. Senior[a,b], Sabina Anwar[a,b], Brent Ryan[a,b], Thierry Deltheil[a,b], Polina Kosillo[a,b], Milena Cioroch[a,b], Katharina Wagner[a,b], Olaf Ansorge[a,d], David M. Bannerman[a,e], J. Paul Bolam[a,c], Peter J. Magill[a,c], Stephanie J. Cragg[a,b], and Richard Wade-Martins[a,b,2]

[a]Oxford Parkinson's Disease Centre [b]Department of Physiology, Anatomy and Genetics, [c]Medical Research Council Anatomical Neuropharmacology Unit, Department of Pharmacology, [d]Nuffield Department of Clinical Neuroscience, John Radcliffe Hospital, and [e]Department of Experimental Psychology, University of Oxford, Oxford OX1 3QX, United Kingdom

Edited by Thomas C. Südhof, Stanford University School of Medicine, Stanford, CA, and approved September 5, 2013 (received for review May 15, 2013)

The pathological end-state of Parkinson disease is well described from postmortem tissue, but there remains a pressing need to define early functional changes to susceptible neurons and circuits. In particular, mechanisms underlying the vulnerability of the dopamine neurons of the substantia nigra pars compacta (SNc) and the importance of protein aggregation in driving the disease process remain to be determined. To better understand the sequence of events occurring in familial and sporadic Parkinson disease, we generated bacterial artificial chromosome transgenic mice (*SNCA*-OVX) that express wild-type α-synuclein from the complete human *SNCA* locus at disease-relevant levels and display a transgene expression profile that recapitulates that of endogenous α-synuclein. *SNCA*-OVX mice display age-dependent loss of nigrostriatal dopamine neurons and motor impairments characteristic of Parkinson disease. This phenotype is preceded by early deficits in dopamine release from terminals in the dorsal, but not ventral, striatum. Such neurotransmission deficits are not seen at either noradrenergic or serotoninergic terminals. Dopamine release deficits are associated with an altered distribution of vesicles in dopaminergic axons in the dorsal striatum. Aged *SNCA*-OVX mice exhibit reduced firing of SNc dopamine neurons in vivo measured by juxtacellular recording of neurochemically identified neurons. These progressive changes in vulnerable SNc neurons were observed independently of overt protein aggregation, suggesting neurophysiological changes precede, and are not driven by, aggregate formation. This longitudinal phenotyping strategy in *SNCA*-OVX mice thus provides insights into the region-specific neuronal disturbances preceding and accompanying Parkinson disease.

dopamine transmission | in vivo electrophysiology | voltammetry | neurodegeneration | behavioral phenotyping

The development of new disease-modifying therapies for Parkinson disease (PD) is critically dependent on animal models that accurately recapitulate pathophysiological sequelae in an age-dependent manner. The generation of such models using genetically altered animals has proved challenging. The traditional use of heterologous gene promoters in the generation of transgenic mouse models precluded an endogenous transgene expression profile and produced additional phenotypes that are not characteristic of PD (1). In contrast, bacterial artificial chromosome (BAC) technology can enable expression of a desired transgene under the control of its native promoter and regulatory elements to achieve a correct spatiotemporal expression profile, thereby providing a more physiological model for investigating molecular mechanisms of the disease.

The α-synuclein gene (*SNCA*) has been implicated in PD through three dominant point mutations (2–4) and locus multiplication (5, 6). *SNCA* duplications and triplications cause autosomal-dominant PD in which the age of onset and disease severity are related in a gene dosage-dependent manner (5, 6). More recently, genome-wide association studies (GWASs) have demonstrated a link between common *SNCA* variants and sporadic forms of PD, with disease-associated polymorphisms proposed to increase α-synuclein (α-syn) expression either by increasing transcription or stabilizing mRNA (7–9). Although α-syn aggregation into cytoplasmic Lewy bodies is seen in human PD patient postmortem tissue, it is not known whether neurophysiological dysfunction and cell death precede the formation of aggregates.

To better understand the mechanisms by which elevated α-syn leads to the progressive neuronal dysfunction seen in PD, we have generated BAC transgenic mice (*SNCA*-OVX) that express human wild-type α-syn at twice the endogenous level of mouse α-syn. Using a longitudinal "deep phenotyping" strategy in these *SNCA*-OVX mice, in vitro and in vivo, we find disturbances to midbrain dopamine neuron function at discrete phases that precede and/or accompany PD-like loss of dopamine neurons and motor deficits. Specifically, dopamine transmission and vesicular organization are compromised selectively in dorsal striatum before a subsequent loss of dopamine neurons, abnormal firing in remaining dopamine neurons in vivo, and movement deficits. These findings thus provide key insights into the progression of events in PD.

Results

Molecular Characterization of *SNCA*-OVX Mice. We generated *SNCA* transgenic mice using a BAC construct carrying the complete

Significance

Elevated expression of the presynaptic protein α-synuclein underlies familial and sporadic Parkinson disease (PD). However, our understanding of how increases in α-synuclein levels drive the sequence of events leading to PD is incomplete. Here, we apply a multidisciplinary longitudinal analysis to a new α-synuclein transgenic mouse model. We show that early-stage decreases in dopamine release and vesicle reclustering precede late-stage changes in neuronal firing properties, measured by in vivo recordings from vulnerable neurons. Accumulated deficits in dopamine neurotransmission and altered neuronal firing are associated with cell death and motor abnormalities, in the absence of protein aggregation in the substantia nigra. These findings have important implications for developing therapies.

Author contributions: O.A., D.M.B., J.P.B., P.J.M., S.J.C., and R.W.-M. designed research; S.J., S.T., P.D.D., M.J.D., T.N.T., D.P., L.P., S.L.S., S.A., B.R., T.D., P.K., M.C., and K.W. performed research; S.J., S.T., P.D.D., M.J.D., T.N.T., D.P., L.P., B.R., T.D., D.M.B., J.P.B., P.J.M., S.J.C., and R.W.-M. analyzed data; and S.J., S.T., P.D.D., J.P.B., P.J.M., S.J.C., and R.W.-M. wrote the paper.

The authors declare no conflict of interest.

This article is a PNAS Direct Submission.

Freely available online through the PNAS open access option.

[1]S.J., S.T., and P.D.D. contributed equally to this work.

[2]To whom correspondence should be addressed. E-mail: richard.wade-martins@dpag.ox.ac.uk.

This article contains supporting information online at www.pnas.org/lookup/suppl/doi:10.1073/pnas.1309143110/-/DCSupplemental.

111-kb wild-type human *SNCA* locus (Fig. S1*A*). Two mouse lines were generated: *SNCA*-OVX, which overexpresses human α-syn to levels that model those associated with *SNCA* multiplications (10), and hα-syn, which expresses human α-syn at a low/moderate level as a control for expression of human α-syn. Both lines were bred to a mouse α-syn-null ($Snca^{-/-}$) pure C57/Bl6 background (11) to preclude confounding interactions with endogenous α-syn. Complete transgene integration was confirmed by exon PCR amplification of all six human *SNCA* exons (Fig. S1*B*). For *SNCA*-OVX mice, a single site of integration was identified by

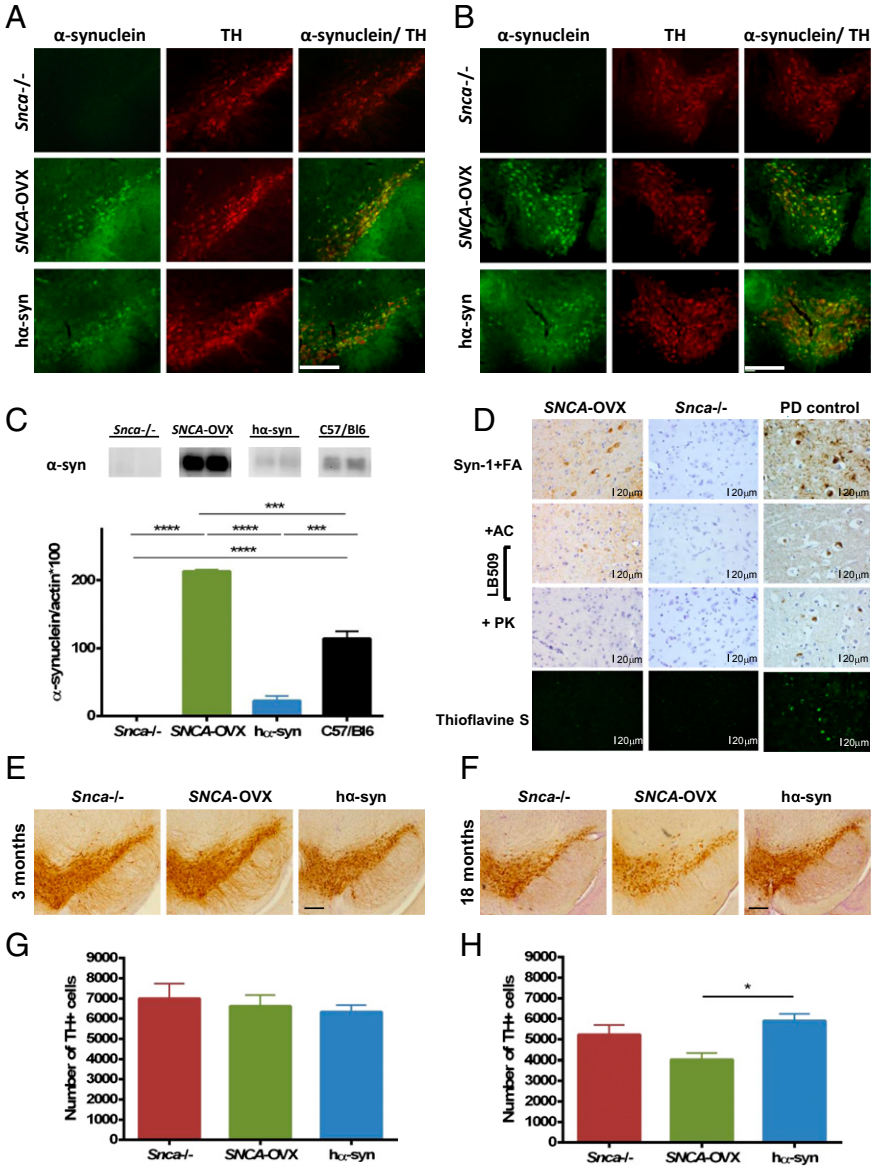

Fig. 1. Characterization of α-syn transgenic mice. (*A and B*) Double immunofluorescence labeling for α-syn and TH confirms human α-syn transgene expression in TH-immunoreactive dopamine neurons of the (*A*) SNc and (*B*) VTA in 3-mo-old *SNCA*-OVX and hα-syn animals. (Scale bars, 200 μm.) (*C*) Quantitative Western analysis of striatal α-syn expression in 3-mo-old *SNCA*-OVX, hα-syn, $Snca^{-/-}$, and C57/Bl6 animals reveals that *SNCA*-OVX animals express the human wild-type *SNCA* transgene at 1.9-fold higher levels compared with endogenous mouse α-syn protein in C57/Bl6 animals. No α-syn expression was observed in $Snca^{-/-}$ control animals. One-way ANOVA with Bonferroni post hoc analysis; $^{****}P < 0.0001$, $^{***}P < 0.001$, $n = 2$–3. (*D*) Immunohistochemical analysis revealed somatic cytoplasmic α-syn immunostaining in cells of the SNc in 18-mo-old *SNCA*-OVX mice using the Syn-1 antibody with formic acid (FA) pretreatment. Similar structures were weakly labeled in 18-mo-old *SNCA*-OVX mice using the LB509 antibody autoclaved (AC) in citric buffer. This staining was abolished when proteinase K (PK) antigen retrieval was applied instead. All of these immunohistochemical stainings were carried out together with control tissue (entorhinal cortex from a PD patient with dementia that shows prominent Lewy body and neuritic pathology). No "amyloid" pathology was detected with thioflavine S in either 18-mo-old *SNCA*-OVX or $Snca^{-/-}$, whereas several Lewy bodies and dystrophic neurites were detected in the positive PD control. (Scale bars, 20 μm; magnification: all pictures, 400×.) (*E* and *G*) At 3 mo of age, stereological cell counting revealed no differences in the number of TH-immunoreactive neurons in the SNc of *SNCA*-OVX mice compared with hα-syn and $Snca^{-/-}$ mice. One-way ANOVA: no main effect of genotype: $F < 1$, $P > 0.05$, $n = 5$ per genotype. Data are expressed as the mean ± SEM. Representative images of TH-immunoreactivity in the SNc are shown. (Scale bar, 200 μm.) (*F* and *H*) Analysis of 18-mo-old animals revealed a 30% loss of TH-immunoreactive neurons in the SNc of *SNCA*-OVX mice compared with hα-syn mice. One-way ANOVA with Bonferroni post hoc analysis: main effect of genotype: $F_{(2,12)} = 6.3$, $^{*}P < 0.05$, $n = 5$ per genotype. Data are expressed as the mean ± SEM. Representative images of TH immunoreactivity in the SNc are shown. (Scale bar, 200 μm.)

fluorescence in situ hybridization analysis near the centromere of chromosome 4 and, for hα-syn mice, a single site near the telomere of chromosome 2 (Fig. S1*C*).

Double immunofluorescence labeling for tyrosine hydroxylase (TH) and α-syn revealed transgene expression in TH-immunoreactive dopamine neurons in the substantia nigra pars compacta (SNc) (Fig. 1*A*) and ventral tegmental area (VTA) (Fig. 1*B*) of *SNCA*-OVX and hα-syn (but not *Snca*$^{-/-}$) mice. Transgene expression was also found to recapitulate the regional expression pattern of endogenous mouse α-syn in other brain regions including cortex, hippocampus, and striatum (Fig. S1*E*). Human α-syn levels in the striatum of *SNCA*-OVX mice were 1.9-fold higher relative to the levels of endogenous mouse α-syn in age-matched C57/Bl6 animals (Fig. 1*C*). We observed no change in β-synuclein or γ-synuclein levels in *SNCA*-OVX mice (Fig. S1*D*).

Soluble high-molecular-weight α-syn species were observed in the midbrain of *SNCA*-OVX mice at both 3 and 18 mo of age, but not in hα-syn mice, as assessed by native PAGE (Fig. S2*A*). The absence of soluble high-molecular-weight species in hα-syn mice was confirmed by loading increasing amounts of protein, such that the levels of α-syn in the samples were comparable, without the appearance of the smear of higher-molecular-weight species being seen. In addition, it was confirmed that these soluble species were similar to those observed in PD, by comparison with SNc tissue from a PD patient. A C-terminal truncated form of α-syn was observed at low levels in the midbrain of 18-mo-old *SNCA*-OVX mice, as demonstrated by Western blotting with an antibody raised against the central portion (aa 18–123) of α-syn followed by reprobing with an antibody raised against the C terminus (aa 118–123) of α-syn (Fig. S2*B*). This truncation generated a fragment comparable in size to that observed in the SNc of a PD patient but was not observed in hα-syn mice or in any of the samples probed with the C-terminal antibody. No evidence of α-syn phosphorylation at S129 was observed in any of the mice strains using a number of commercial S129P antibodies (Fig. S2*C*).

We looked for the presence of pathological α-syn aggregates in the *SNCA-OVX* line at 18 mo of age. Proteinase K treatment, which enhances the immunoreactivity of "abnormal" α-syn (i.e., that in intracytoplasmic aggregates) and also diminishes that of diffuse physiological expression (12), abolished the immunoreactivity of α-syn in the SNc (Fig. 1*D*) and striatum (Fig. S3*A*) of aged *SNCA*-OVX mice. Similarly, thioflavine S, which detects the β-sheet–rich amyloid and p62, a common constituent in several types of disease-associated inclusions, revealed no pathological protein aggregations in the SNc of *SNCA*-OVX mice (Fig. S3*B*). No qualitative differences in astrogliosis or microglial activation were detected between *SNCA*-OVX mice and *Snca*$^{-/-}$ controls, as analyzed by immunohistochemistry using antibodies against GFAP and Iba-1, respectively (Fig. S3*B*). Hyperphosphorylated tau (AT8) and β-amyloid (4G8) staining was negative in all animals (Fig. S3*B*).

Aged *SNCA*-OVX Animals Lose Nigrostriatal Dopamine Neurons. To assess whether progressive degeneration of SNc dopamine neurons, a cardinal pathological feature of PD, occurs as a consequence of overexpressing α-syn, an unbiased stereological count of TH-immunoreactive neurons was performed in the SNc of 3- and 18-mo-old mice. It is already known that *Snca*$^{-/-}$ mice display a small decrease in dopamine neurons (13, 14); therefore, to evaluate the effects of increased levels of α-syn we compared the number of dopamine neurons in *SNCA*-OVX to those in hα-syn mice. In young adults (3 mo), no difference was found in the number of TH-immunoreactive neurons between genotypes (Fig. 1 *E* and *G*). However, in aged mice (18 mo), *SNCA*-OVX animals displayed a 30% reduction in TH-immunoreactive neurons in the SNc compared with the hα-syn mice (Fig. 1 *F* and *H*). At 18 mo of age, *SNCA*-OVX animals also displayed a 22% reduction in hematoxylin-counterstained neurons in the SNc compared with the hα-syn mice (Fig. S4*B*), whereas no difference in hematoxylin-stained cells was observed at 3 mo of age (Fig. S4*A*), confirming that the loss of TH-immunoreactive neurons in aged *SNCA*-OVX mice was not due to a down-regulation of TH expression. The loss of SNc dopamine neurons in aged *SNCA*-OVX mice was observed in the absence of overt aggregation pathology in the SNc and striatum, suggesting α-syn aggregation is not required for neuronal death in the SNc.

SNCA-OVX Mice Display Early Nonmotor and Late Motor Phenotypes. *SNCA*-OVX and control mice were analyzed for nonmotor phenotypes that reflect early symptoms of PD. We assessed gastrointestinal function and revealed an increased dry stool weight in male *SNCA*-OVX mice that was independent of age (Fig. 2*A*). This increase in dry stool weight was not accompanied by an increased stool frequency or stool water content (Fig. S5 *A* and *B*), indicating a constipation-like phenotype that was seen in male, but not female, *SNCA*-OVX mice.

We next assessed motor function using the accelerating rotarod, multiple static rods, and the forepaw stride length tests. On the rotarod test, the latency of aged (18 mo) but not young (3 mo) *SNCA*-OVX mice to fall was significantly reduced compared with hα-syn and *Snca*$^{-/-}$ controls (Fig. 2*B*). *SNCA*-OVX animals at 18 mo of age were also impaired on the multiple static rods test (Fig. 2 *C–E* and Movies S1 and S2) compared with age-matched controls. *SNCA*-OVX mice also displayed a reduced forepaw stride length compared with littermate control *Snca*$^{-/-}$ mice (Fig. 2*F*). *SNCA*-OVX mice did not display differences in latency to fall in the inverted screen test compared with age-matched hα-syn and *Snca*$^{-/-}$ controls, indicating that poor performance in the rotarod and multiple static rods tests was due to impaired motor coordination rather than muscle weakness (Fig. S5*C*).

Early and Sustained Deficits in Dopamine Transmission in the Dorsal Striatum of *SNCA*-OVX Mice. Having established a mouse model that displays an age-dependent Parkinsonian phenotype, we sought to investigate what changes might precede or accompany the phenotypic alterations. In PD, the nigrostriatal dopamine neurons projecting from the SNc to the dorsal striatum [caudate putamen (CPu)], are preferentially affected compared with mesolimbic dopamine neurons projecting from the VTA to the ventral striatum [nucleus accumbens (NAc)]. Expression of the α-syn transgene was confirmed in both the CPu and NAc of *SNCA*-OVX transgenic mice (Fig. S6 *A* and *B*). To investigate region- and age-dependent changes in dopamine transmission in *SNCA*-OVX mice, we used fast-scan cyclic voltammetry (FCV) at carbon-fiber microelectrodes, which detects dopamine release and reuptake in real time. In the dorsal striatum, mean peak extracellular concentrations of dopamine ($[dopamine]_o$) evoked by single electrical pulses across distributed recording sites were, on average, ~30% lower in *SNCA*-OVX mice than in littermate *Snca*$^{-/-}$ controls (Fig. 3 *A–C*, left traces). This reduced release was present from a young age (3–4 mo) before the loss of dopamine neurons (Fig. 1*H*) and persisted throughout the lifespan of adult mice (tested at 3–4, 12, and 18 mo). The greatest deficits were found in dorsal and lateral recording sites (Fig. 3*G*). In contrast, in the ventral striatum no significant difference in evoked $[dopamine]_o$ was detected between the two genotypes at any time point (Fig. 3 *A–C*, right traces).

In young and aged hα-syn mice, mean peak $[dopamine]_o$ evoked by single pulses in CPu or NAc was not significantly different from that in *Snca*$^{-/-}$ littermates (Fig. 3 *H* and *I*), suggesting that the deficit in evoked $[dopamine]_o$ in *SNCA*-OVX mice was a consequence of the elevated levels of human α-syn rather than its expression per se. Dopamine content of CPu or

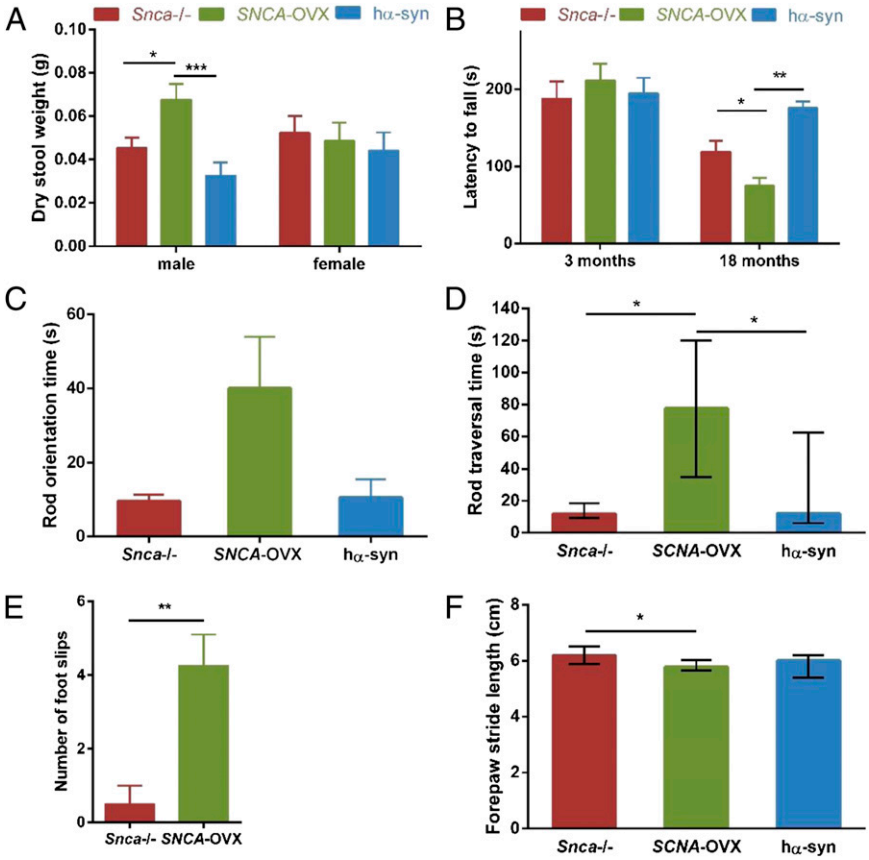

Fig. 2. Early nonmotor and late motor phenotypes in *SCNA*-OVX mice. (*A*) Male *SNCA*-OVX animals displayed an increased dry stool weight independent of age. Three-way ANOVA; main effect of age: $F_{(1,84)} = 20.66$, $^{****}P < 0.0001$; genotype/sex interaction: $F_{(2,83)} = 3.19$, $^{*}P < 0.05$; no interaction between genotype and age: $F_{(2,83)} = 1.44$, $P > 0.05$; separate ANOVA for males: main effect of genotype: $F_{(2,45)} = 7.76$, $^{***}P < 0.001$ (Tukey post hoc test $^{*}P < 0.05$, $^{***}P < 0.001$), $n = 4$–11; females: main effect of genotype: $F < 1$, $P > 0.05$, $n = 3$–8. Data are expressed as mean ± SEM. (*B*) Rotarod performance was impaired in 18- but not in 3-mo-old *SNCA*-OVX mice. Two-way ANOVA of square-root transformed data: main effect of age: $F_{(1,28)} = 25.95$, $^{***}P < 0.001$; main effect of genotype: $F_{(2,27)} = 3.49$, $^{*}P < 0.05$; genotype/age interaction: $F_{(2,27)} = 6.14$, $^{**}P < 0.01$; separate ANOVAs revealed no main effect of genotype at 3 mo ($F < 1$, $P > 0.05$), but a significant main effect of genotype at 18 mo ($F_{(2,15)} = 10.04$, $^{**}P < 0.01$) (Tukey post hoc test $^{*}P < 0.05$, $^{**}P < 0.01$), $n = 3$–8), which remained significant when body weight was included as a covariate (ANCOVA: main effect of genotype: $F_{(2,14)} = 4.93$, $^{*}P < 0.05$). Data are expressed as mean ± SEM. (*C*–*E*) *SNCA*-OVX animals (18 mo old) were impaired on the multiple static rods test compared with hα-syn and *Snca*$^{-/-}$ animals. (*C*) Orientation: ANOVA of square-root transformed data collapsed across both rods; main effect of genotype: $F_{(2,24)} = 3.35$, $P = 0.05$, $n = 7$–10. Data are expressed as mean ± SEM. (*D*) Traversing: Kruskal–Wallis one-way ANOVA on ranked data collapsed across both rods. Effect of genotype: $H_2 = 12.37$; $^{**}P < 0.01$ (Dunn's post hoc pairwise comparison $^{*}P < 0.05$), $n = 7$–10. Data are expressed as median ± IQ range. (*E*) *SNCA*-OVX animals displayed increased foot slips when traversing rod 2 ($^{**}P < 0.01$, Welch *t* test: $t = 3.79$, df = 6, $n = 4$ per group). Rods had a diameter of 22 mm (rod 1) and 9 mm (rod 2). (*F*) *SNCA*-OVX animals displayed reduced stride length compared with *Snca*$^{-/-}$ mice (Kruskal–Wallis one-way ANOVA on ranked data, comprising data from both ages and sexes: main effect of genotype: $H_{(2)} = 10.79$, $^{**}P < 0.01$ (Dunn's post hoc pairwise comparison $^{*}P < 0.05$), $n = 15$–30). Data are expressed as median ± IQ range.

NAc assessed by HPLC was not significantly different between hα-syn and *Snca*$^{-/-}$ mice at either 3 or 18 mo (Fig. 3 *J* and *K*). Because no phenotypic changes were detected in hα-syn mice compared with *Snca*$^{-/-}$ mice, our subsequent analyses focused on comparing *SNCA*-OVX transgenic mice with their littermate control *Snca*$^{-/-}$ mice.

Lower levels of evoked $[\text{dopamine}]_o$ in dorsal striatum of *SNCA*-OVX compared with *Snca*$^{-/-}$ mice were not due to reduced striatal dopamine content: HPLC analysis showed net dopamine content was unchanged in CPu or NAc in *SNCA*-OVX compared with *Snca*$^{-/-}$ mice at 3–4 and 12 mo (Fig. 3 *D* and *E*), whereas at 18 mo dopamine content in CPu (but not NAc) was, paradoxically, greater in *SNCA*-OVX mice compared with *Snca*$^{-/-}$ controls, and unaltered in NAc (Fig. 3*F*). Furthermore, apparent deficits in dopamine release in dorsal CPu of either young or aged adult *SNCA*-OVX mice were not due to diminished $[\text{dopamine}]_o$ that might result from enhanced dopamine uptake, because dopamine uptake kinetics were normal (Fig. S6*C*). No change in the level of dopamine transporter protein was observed (Fig. S6*D*). In addition, we excluded a role for striatal ACh input to dopamine axons from cholinergic interneurons, which play a key role in driving dopamine release probability (15): A dopamine release deficit persisted in the presence of nicotinic receptor blockade by dihydro-β-erythroidine (Fig. S6 *E* and *F*). There were also no detectable changes in the net dependence on extracellular Ca^{2+} (Fig. S6*G*).

No Change in SNARE Complex Formation but Changes in Dopamine Vesicle Distribution. We next sought to understand the underlying molecular, neuroanatomical, and neurophysiological changes in the SNc that may lead to progressive neuronal loss in the *SNCA*-OVX model of PD. The reduction in evoked $[\text{dopamine}]_o$ seen before loss of dopamine neurons or dopamine content suggests a reduction in the releasability of dopamine. However, we found no differences in SNARE complex formation in the striatum of 6-mo-old *SNCA*-OVX mice compared with age-matched controls (Fig. S7 *A* and *B*) or any changes in the striatal protein levels of SNAP25, VAMP2, complexins, or synapsins (Fig. S7 *C*–*G*). These

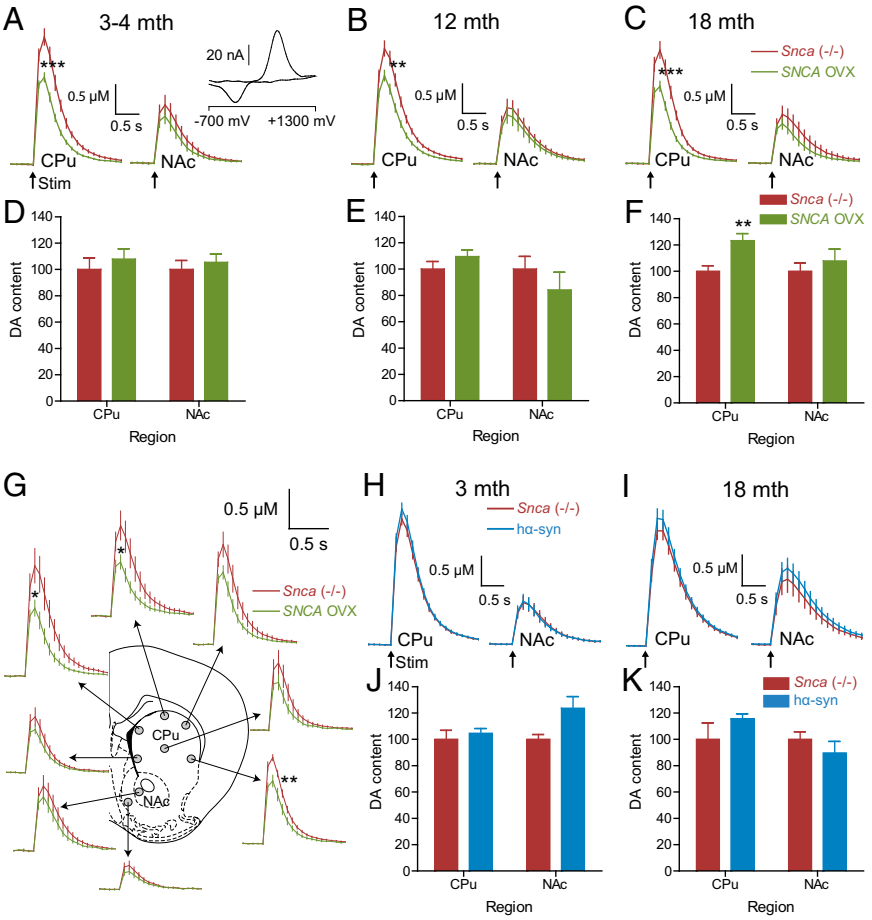

Fig. 3. α-syn overexpression limits dopamine release from an early age in CPu, but not NAc. (*A–C*) Mean extracellular dopamine concentration ($[dopamine]_o$) profiles vs. time (mean ± SEM) following single pulse stimulation (↑200 μs, 0.6 mA) in CPu (*A–C*, left traces) or NAc (*A–C*, right traces) of *Snca*$^{-/-}$ vs. *SNCA*-OVX at increasing ages. Mean peak evoked $[dopamine]_o$ was significantly lower in *SNCA*-OVX compared with *Snca*$^{-/-}$ in CPu (**$P < 0.01$, ***$P < 0.001$; unpaired *t* test; $n = 60–72$) but not NAc ($P > 0.05$; unpaired *t* test; $n = 19–23$) at 3–18 mo. (*D–F*) Dopamine content (expressed as a percentage of *Snca*$^{-/-}$) in CPu and NAc dissected from striatal slices used for FCV recordings. Mean dopamine content was not significantly different between *SNCA*-OVX and *Snca*$^{-/-}$ in CPu or NAc ($P > 0.05$, unpaired *t* test, $n = 10$) between ages 3 and 12 mo. However, at 18 mo mean dopamine content was significantly greater in CPu of *SNCA*-OVX compared with *Snca*$^{-/-}$ (*F*; **$P < 0.01$, unpaired *t* test, $n = 12$) but not NAc. (*G*) Typical FCV recording sites include six CPu and two NAc recordings. Mean peak $[dopamine]_o$ from individual sites from 3- to 4-mo-old *Snca*$^{-/-}$ and *SNCA*-OVX highlights more prominent $[dopamine]_o$ deficit in dorsal striatum (ventrolateral striatum **$P < 0.01$; dorsomedial and dorso-mid striatum *$P < 0.05$; all other regions $P > 0.05$; unpaired *t* test; $n = 10–14$ per region). (*H* and *I*) The hα-syn mice show no difference compared with *Snca*$^{-/-}$ mice in mean peak evoked $[dopamine]_o$ ($P > 0.05$; unpaired *t* test; *H*: 3 mo, $n = 18$ NAc, $n = 60$ CPu; *I*: 18 mo, $n = 15$ NAc, $n = 47$ CPu) or dopamine content ($P > 0.05$; unpaired *t* test; *J*: 3 mo, $n = 10$; *K*: 18 mo, $n = 7$) in CPu or NAc. Absolute values for dopamine content ranged from 97 to 240 pmol/mm^3 tissue in CPu to 47–104 pmol/mm^3 tissue in NAc.

results are consistent with previous finding that striatal SNARE complex formation in striatum is not regulated by synucleins (16).

We next explored the alternative hypothesis that α-syn might restrict dopamine release by altering the distribution of the vesicular pool in dopamine axons in the dorsal striatum (17). We used electron microscopy to analyze the structure of TH-immunoreactive synaptic and nonsynaptic axonal profiles in the CPu of 3-mo-old *SNCA*-OVX and *Snca*$^{-/-}$ mice. The mean cross-sectional area of profiles, the number and density of vesicles per profile, and the distance of vesicles to the plasma membrane were similar in both genotypes (Table S1). When a synapse was present, there were also no differences in the synaptic membrane length or distance of vesicles to the active zone. However, vesicles in *SNCA*-OVX mice were more clustered than those in *Snca*$^{-/-}$ mice; the frequency distribution of intervesicle distance was significantly different between genotypes ($P < 0.0001$; two-sample Kolmogorov–Smirnov test; Fig. 4), and vesicles were three times less dispersed in *SNCA*-OVX mice (index of dispersion $D_{SNCA\text{-}OVX}/D_{Snca^{-/-}} = 0.34$).

Monoamine Neurotransmission Deficit Does Not Extend to Norepinephrine or 5-Hydroxytryptamine. To determine whether the deficit in dopamine release in the dorsal striatum of *SNCA*-OVX mice is seen for other amines elsewhere, we investigated the release of norepinephrine (NE) and 5-hydroxytryptamine (5-HT) from axon terminals in innervation-rich areas, the bed nucleus of the stria terminalis (BNST) and substantia nigra pars reticulata (SNr), respectively. We confirmed transgene expression in the cell soma regions, the locus coeruleus and the dorsal raphe nucleus, in *SNCA*-OVX mice by immunohistochemistry (Fig. S8). Mean peak extracellular concentrations of NE ($[NE]_o$) in the ventromedial portion of the BNST (Fig. 5 *A* and *B*) evoked by stimulus trains of 30 pulses at 10, 25, 50, and 100 Hz in *SNCA*-OVX mice were not different from those in *Snca*$^{-/-}$ mice irrespective of age (3 or 18 mo; Fig. 5 *C–F*). Similarly, mean peak extracellular concentrations of 5-HT ($[5\text{-HT}]_o$) in SNr (Fig. 5 *G* and *H*) evoked by stimulus trains of 20 or 40 pulses at 50 Hz in *SNCA*-OVX mice were not different from those in *Snca*$^{-/-}$ mice at either young (3 mo, Fig. 5 *I* and *J*) or old age (18 mo, Fig. 5 *K* and *L*). These data show that α-syn overexpression does not

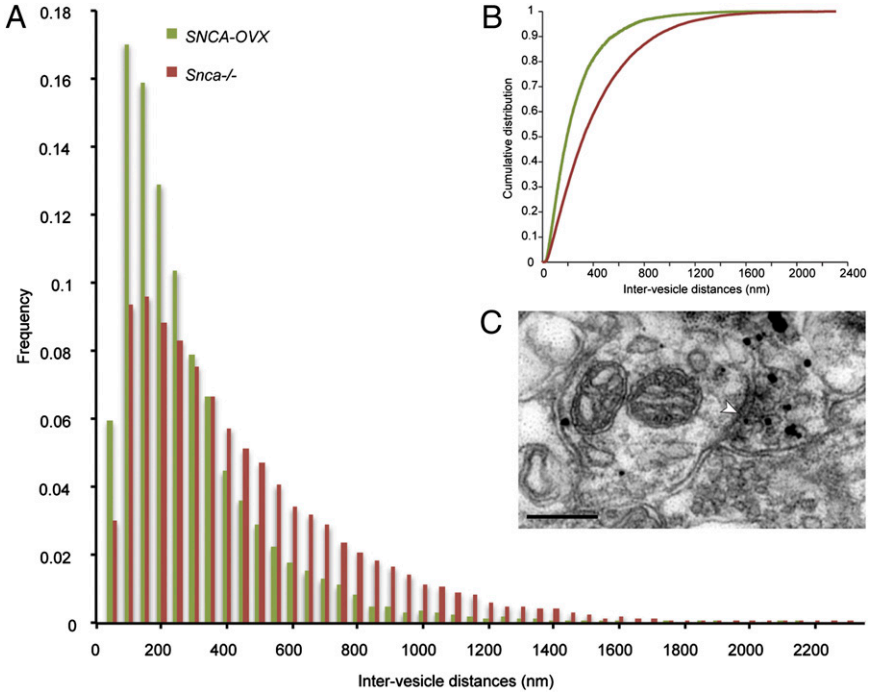

Fig. 4. Overexpression of α-syn alters vesicle clustering in dopaminergic synaptic boutons in the dorsal striatum. (*A*) Frequency distribution of intervesicle distance in TH-immunoreactive profiles in the striatum of *SNCA-OVX* and *Snca*$^{-/-}$ mice. The two-sample Kolmogorov–Smirnov test was performed to test for differences between the two distributions and revealed a significant difference between the groups (****$P < 0.0001$). (*B*) Cumulative distribution functions of the two data groups. Application of an index of dispersion, $D = \sigma^2/\mu$, to each raw dataset ($D_{SNCA\text{-}OVX}$, $D_{Snca}{}^{-/-}$) shows that the *Snca*$^{-/-}$ vesicles are three times more dispersed than the *SNCA-OVX* ($D_{SNCA\text{-}OVX}/D_{Snca}{}^{-/-} = 0.34$). (*C*) Electron micrograph of a TH immunogold-labeled axon terminal in the dorsal striatum identified by the accumulation of electron dense silver-intensified immunogold particles. The bouton forms symmetrical synaptic contact (arrowhead) with a dendritic shaft. Note the accumulation of vesicles within the bouton. (Scale bar, 0.2 μm.)

affect the axonal release of 5-HT or NE, further suggesting that the neurotransmission deficit in *SNCA*-OVX mice is highly selective for cell type and brain circuit.

SNc Dopamine Neurons in *SNCA*-OVX Mice Exhibit Age-Dependent Reductions in Firing Rates in Vivo. To gain further insight into the pathophysiological sequelae of α-syn overexpression in midbrain dopamine systems, we tested for changes in the action potential firing properties of SNc dopamine neurons in vivo. We made extracellular recordings from individual SNc neurons in young and aged (3–4 and 18–22 mo) anesthetized *SNCA*-OVX mice and their *Snca*$^{-/-}$ littermates (Fig. 6). After recording, we juxtacellularly labeled each neuron with Neurobiotin (18) to confirm its dopamine phenotype (TH immunoreactivity) and location in SNc, as well as test for their expression of α-syn (Fig. 6 *A* and *C*; all recorded dopamine neurons ($n = 43$) from *SNCA*-OVX mice expressed the α-syn transgene). In young *SNCA*-OVX and *Snca*$^{-/-}$ mice, the firing rates and action potential durations of SNc dopamine neurons were similar (Fig. 6*E*). Moreover, neurons in both genotypes exhibited similar coefficients of variation (a measure of regularity of firing) and propensities to fire in a "regular," "irregular," or "bursty" pattern (Fig. 6*G* and *SI Materials and Methods*). Thus, in young adult animals at least, α-syn overexpression does not alter these key firing properties of SNc dopamine neurons. However, for SNc dopamine neurons recorded in the aged *SNCA*-OVX and *Snca*$^{-/-}$ mice (Fig. 6 *B* and *D*), we found a significant reduction (nearly 30%) in the firing rate, but no change in the firing patterns, of dopamine neurons in *SNCA*-OVX mice (Fig. 6 *F* and *H*). Taken together, these data show that overexpression of human α-syn does not compromise key firing properties of SNc dopamine neurons in young adulthood but significantly reduces the firing rates of these neurons in old age.

Discussion

Here, we describe the generation and longitudinal deep-phenotyping of a unique transgenic model of PD and identify the sequence of disease mechanisms triggered by overexpression of α-syn to levels associated with both familial and sporadic human disease. Using transgenic *SNCA*-OVX mice, we have localized early and selective deficits in dopamine neurotransmission to the nigrostriatal pathway. This early-onset phenotype is followed in aged animals by a pathology of loss of dopamine neurons, reduced SNc dopamine neuron firing rates, and motor impairments. Furthermore, this constellation of Parkinsonian phenotypes caused by elevated α-syn is not dependent on overt protein aggregation but is associated with soluble high-molecular-weight α-syn species observed at 3 and 18 mo of age in *SNCA*-OVX mice.

Our use of BAC transgenesis to overexpress human wild-type α-syn from the complete human genomic DNA locus driven by the endogenous promoter helped ensure correct spatiotemporal regulation of expression, reflecting endogenous α-syn expression. Overexpression of α-syn is a likely mechanism underlying both rare familial PD, caused by *SNCA* duplications and triplications (5, 6), and sporadic PD (19). PD-associated variants at the *SNCA* locus, identified by GWAS, are proposed to enhance expression by either increasing *SNCA* transcription or enhancing mRNA stability (9). The *SNCA*-OVX mouse therefore acts as a model of both familial and sporadic PD. The *SNCA*-OVX line expresses the *SNCA* transgene at 1.9-fold the levels of endogenous mouse α-syn; this near-doubling mirrors the change in human α-syn levels that result from a triplication of the *SNCA* locus in familial PD (10). Elevated levels of α-syn have previously also been demonstrated in sporadic cases of PD in which remaining dopamine midbrain neurons from patients with sporadic disease show up to a sixfold increase in α-syn mRNA levels (19).

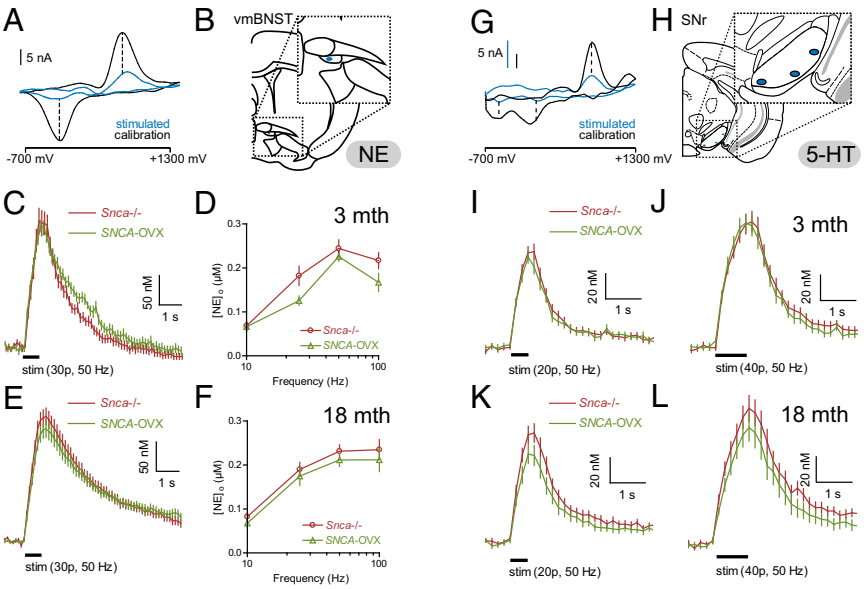

Fig. 5. α-syn overexpression does not alter nondopamine amine signaling in bed nucleus of the stria terminalis and substantia nigra pars reticulata. (*A*) Typical cyclic voltammograms from electrically evoked recordings of NE in BNST (stimulated) and following calibration in 2 μM NE (calibration). Note single oxidation and reduction current peaks at +560–580 and −200 mV, respectively. (*B*) Typical recording site in ventromedial portion of BNST (vmBNST) ∼0.26 mm anterior of bregma. Mean profiles of extracellular NE concentration ($[NE]_o$) vs. time (mean ± SEM) following train stimulation (30 pulses, 50 Hz) in vmBNST in young adult (*C*) (3 mo, n = 33–35) or aged adult (*E*) (18 mo, n = 70–74) $Snca^{-/-}$ vs. *SNCA*-OVX mice. Mean peak $[NE]_o$ vs. frequency during 30 pulse trains (10–100 Hz) in vmBNST in young adult (*D*) (n = 33–35) or aged adult (*F*) (n = 70–74). (*G*) Typical cyclic voltammograms from electrically evoked recordings of 5-HT in SNr (stimulated) and following calibration in 0.5 μM 5-HT (calibration). Note single oxidation and dual reduction current peaks at approximately +600, −20, and −670 mV, respectively. (*H*) Typical recording sites in the SNr ∼3.2 mm posterior of bregma. Note recording sites located on ventral side of SNr to minimize any possible contribution of dendritic dopamine in recordings. Mean profiles of $[5\text{-HT}]_o$ vs. time following 50-Hz train stimulation (*I*: 20 pulses or *J*: 40 pulses; n = 31–44) in the SNr in young adult (3 mo) and aged adult (18 mo) (*K*: 20 pulses or *L*: 40 pulses; n = 26–32) $Snca^{-/-}$ vs. *SNCA*-OVX mice.

Our study is unique in defining the effect of disease-relevant α-syn overexpression on neurotransmission and vesicle organization in the dopamine pathways most vulnerable in PD. We find an early and sustained deficit in neurotransmission specific to dopamine (rather than the other monoamines, NE and 5-HT). Furthermore, this deficit was localized to the dopamine inputs to dorsal striatum. These findings are reminiscent of our previous work on α-and γ-synuclein double-knockout and α-, β-, γ-synuclein triple-knockout mice, in which we showed that synucleins negatively regulate dopamine release in the dorsal but not ventral striatum (16, 20).

At time points before 18 mo of age, we observed no change in striatal dopamine content, despite a decrease in release. This is consistent with a redistribution, rather than a reduction, of dopamine at release sites. In support of this, we identified increased clustering of vesicles in dopamine terminals in the dorsal striatum of *SNCA*-OVX animals at 3 mo.

Whether the in vivo firing properties of SNc dopamine neurons change before protein aggregation and/or cell death has been a critical, unaddressed issue in PD. We show here that the activity of neurochemically identified SNc dopamine neurons is altered in an age- and genotype-dependent manner. Because midbrain dopamine neurons collectively innervate all basal ganglia nuclei (21), any change in their firing rate or pattern is likely to profoundly disturb the activity of the whole basal ganglia network; it is these disturbances that ultimately underlie the motor symptoms of PD. We found that the spontaneous firing rates of SNc dopamine neurons were reduced by nearly 30% in aged animals overexpressing α-syn. This decrease in spontaneous firing rates, together with dopamine neuron loss and a sustained deficit in striatal dopamine release, may collectively tip the balance toward a greatly reduced dopamine output that can no longer be compensated for, thus resulting in motor impairments in aged animals. It is not clear whether the reduced firing rates of dopamine neurons are a response to alterations in either their inputs or intrinsic properties, or whether this change is, in itself, pathogenic.

The age-related, progressive loss of nigrostriatal dopamine neurons and the presence of α-syn–containing Lewy bodies are the cardinal features of PD pathology. However, the precise relationship between α-syn pathology and dopamine neuron dysfunction and death has been unclear. We show here that dopamine neuronal dysfunction and neuronal death in *SNCA*-OVX mice occurs in the absence of overt protein aggregation pathology in the SNc and striatum but is associated with the presence of soluble high-molecular -weight α-syn species.

In conclusion, we report here a unique transgenic model of PD that exhibits early-onset circuit-specific deficits in dopamine neurotransmission followed subsequently by alterations in neuronal firing properties, a motor phenotype and neuron loss in the absence of overt protein aggregation pathology in the SNc and striatum. We therefore propose that PD-related phenotypes are not driven by progressive protein aggregation, but are associated with much earlier deficits in dopamine neurotransmission. Moreover, movement deficits might emerge when, on a foundation of sustained neurotransmission defects, some dopamine neurons die whereas those remaining decrease their firing. The *SNCA*-OVX mice allow us to advance our understanding of the cellular basis of changes to dopamine and non-dopamine neurotransmission in brain regions that differ in disease susceptibility and provide a model to test next-generation therapies.

Materials and Methods

Generation of Transgenic Mice. Transgenic mouse lines were generated by injection of BAC DNA containing the human wild-type *SNCA* locus into C57/Bl6 mouse pronuclei (Charles River). Transgene integrity and expression levels were analyzed (*SI Materials and Methods*) and two lines were chosen and back-crossed onto an α-syn-null ($Snca^{-/-}$) pure C57/Bl6 background (11) for nine generations to establish two transgenic lines, *SNCA*-OVX and hα-syn. The *SNCA* transgene was maintained in a hemizygous state on a pure

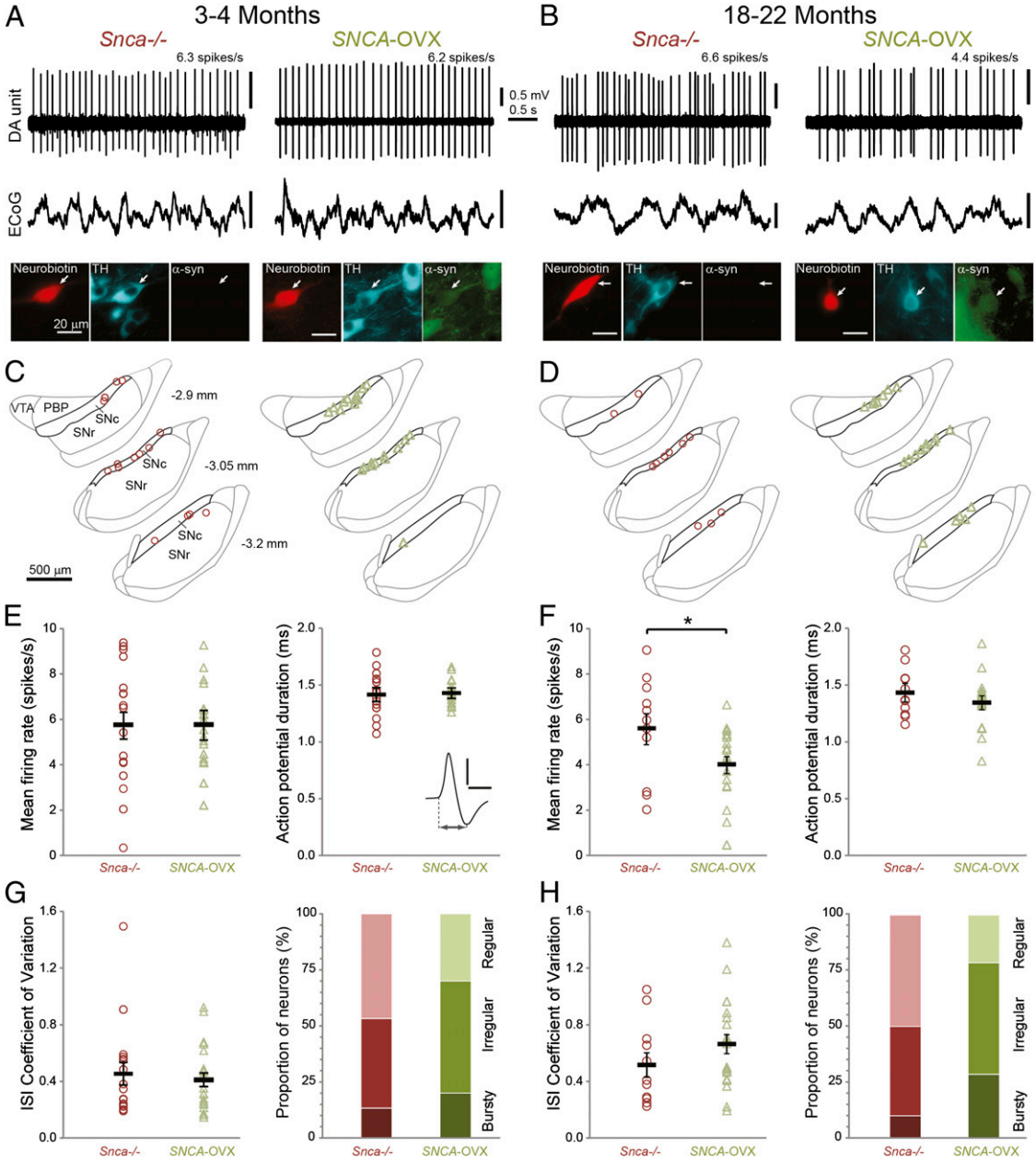

Fig. 6. Spontaneous firing of identified dopaminergic neurons in the substantia nigra in vivo. Unit activity of individual dopamine neurons recorded in (*A*) 3- to 4-mo-old and (*B*) 18- to 22-mo-old *Snca*$^{-/-}$ and *SNCA*-OVX mice during robust slow-wave activity in electrocorticograms (ECoG). Neurons were juxtacellularly labeled with Neurobiotin, verified as dopaminergic by TH expression, and tested for expression of α-syn. (*C* and *D*) Locations of identified dopamine neurons in (*C*) 3- to 4-mo-old and (*D*) 18- to 22-mo-old *Snca*$^{-/-}$ (red) and *SNCA*-OVX (green) mice (dorsal top, lateral right) grouped at three rostro-caudal levels (distances from bregma shown left). PBP, parabrachial pigmented nucleus of the VTA; SNc, substantia nigra pars compacta; SNr, substantia nigra pars reticulata; VTA, ventral tegmental area. [Adapted from ref. 23.] (*E* and *F*) Mean firing rates and action potential durations of SNc dopamine neurons in (*E*) 3- to 4-mo-old (n = 17, *Snca*$^{-/-}$ and 22 neurons, *SNCA*-OVX) and (*F*) 18- to 22-mo-old mice (n = 11 and 21; *$P < 0.05$). (*Inset*) Average wideband-filtered action potential from an *SNCA*-OVX mouse indicating duration measurement (scale 0.5 mV, 1 ms). (*G* and *H*) Mean interspike interval (ISI) coefficients of variation and the proportions of SNc neurons exhibiting each firing mode in (*G*) 3- to 4-mo-old mice (n = 15 and 20 neurons analyzed for mode in *Snca*$^{-/-}$ and *SNCA*-OVX) and (*H*) 18- to 22-mo-old mice (n = 10 and 14 neurons). The firing pattern did not differ significantly with genotype. In *E*–*H*, group means ± SEM are shown in black.

C57/Bl6 background. All procedures were conducted in accordance with the United Kingdom Animals (Scientific Procedures) Act of 1986 and approved by the local ethical review panel at the Department of Physiology, Anatomy and Genetics, University of Oxford.

Immunostaining. Animals were transcardially perfused with PBS (pH 7.4) followed by 4% paraformaldehyde (PFA) (vol/vol). Brains were postfixed in 4% PFA (vol/vol), cryoprotected in 30% sucrose, and sectioned on a freezing microtome (Leica Microsystems). For immunofluorescence, sections (35 μm) were incubated overnight with primary antibodies against α-syn (1:500; Covance) and TH (1:500; Millipore) and then incubated with goat anti-mouse Alexa 488 and goat anti-rabbit Alexa 594 antibody. For peroxidase immunohistochemistry, sections (50 μm) were incubated with primary antibodies against α-syn (1:1,000; BD Bioscience) or TH (1:2,000; Millipore). Sections were incubated with biotinylated secondary antibody followed by incubation in avidin–biotin–peroxidase complex and staining was visualized using 3,3′-diaminobenzidine (DAB). Sections were counterstained with hematoxylin, dehydrated, and coverslipped using DPX Mountant (Fluka Biochemika).

Western analysis. Striatal tissue was homogenized in phosphate buffered saline (pH 7.4) containing 1% (vol/vol) Igepal CA-630, 0.1% (vol/vol) SDS, 0.5% (mass/vol) sodium deoxycholate and protease inhibitor cocktail, using a Tissue Tearor (Biospec Products, Inc). Protein content was quantified using a BAC assay kit (Sigma) and proteins were analyzed by Western blotting. See Table S2 for primary antibodies. Bands were visualized using horseradish peroxidase-conjugated goat anti-mouse IgG (Bio-Rad) and the chemiluminescent ECL+ kit (GE Healthcare). Bands were quantified using ImageJ software. Data was analyzed using one-way ANOVA and Bonferroni post hoc analysis using SPSS Statistics 20 (IBM).

Neuropathology. To detect potential α-syn–related pathology, the mAbs Syn-1 (1:1,000; BD Transduction Labs) against aa 91–99 and LB509 (1:1,000; Invitrogen) against aa115–122 were used. Brains were fixed in 10% formalin (vol/vol), embedded in paraffin, and cut into 6-μm-thick sections, deparaffinized, and rehydrated. Peroxidase activity was eliminated by treatment with 3% H_2O_2 (mass/vol). Antigen retrieval for Syn-1 involved treatment with formic acid for 15 min, and for LB509 involved either autoclaving (121 °C) for 10 min in citrate buffer or treatment with 20 μg/mL proteinase K (Roche) for 10 min at room temperature. The mouse-on-mouse kit (M.O.M.; Vector Labs) was used to minimize the background and staining was visualized using DAB (Vector Labs). Thioflavine S staining was carried out as described by Sun et al. (22).

Stereological Cell Count. The total number of TH-immunoreactive and hematoxylin-counterstained nigral dopamine neurons was estimated with the optical fractionator method of unbiased stereology using the Stereo-Investigator software (MicroBrightField). Sections (50 μm) were processed for TH immunoreactivity as described above. Cells were counted under a 40× objective of a Zeiss Imager M2 microscope using a randomly placed counting frame of 50 × 50 μm on a sample grid of 120 × 160 μm. A 22-μm optical dissector with 2-μm upper and lower guard zones was used. The SNc was delineated using a mouse brain atlas (23). Every second section from 2.7 to 3.88 mm posterior to bregma was counted. Data are expressed as mean number of TH-immunoreactive neurons ± SEM and were analyzed using one-way ANOVA and Bonferroni post hoc analysis using SPSS Statistics 20 (IBM).

Behavior. ***One-hour stool collection.*** Animals (male and female) were placed into separate clean cages and fecal pellets were collected over a 1-h period (1600–1700 hours). Pellets were weighed to obtain wet stool weight, dried overnight at 65 °C, and reweighed to obtain dry stool weight and stool water content (24).

Rotarod. In the rotarod test, female mice were placed on a rod that accelerated from 4 to 40 rpm over a 5-min period. The length of time which the animals were able to stay on the rotating rod was recorded as latency to fall. Animals were tested three times a day for two consecutive days and performance was averaged for each day (20).

Multiple static rods test. In the multiple static rods test, two wooden dowels of 22-mm (rod 1) or 9-mm (rod 2) diameter were clamped to a supporting platform 50 cm above a cushioned surface. Female mice were placed at the end of the rod facing away from the platform. The time taken to turn around by 180° to face the platform, time taken to traverse the rod, and the number of foot slips made when traversing the rod were recorded (20).

Forepaw stride length. In the forepaw stride length test, animals' forepaws were placed in ink and animals walked across a sheet of paper toward their home cage. The distance between steps on the same side of the body, from the middle toe of the first step to the heel of the second step, was measured and averaged to obtain stride length. Only steps during normal walking (straight line, no stopping) were included in the analysis (24). Male and female animals were tested.

Statistics. Data analyzed using a parametric one-, two- or three-way ANOVA followed by a Tukey post hoc test are expressed as means ± SEM. Data analyzed using a nonparametric Kruskal–Wallis ANOVA followed by Dunn's pairwise multiple comparison are expressed as median ± interquartile (IQ) range. Analyses were completed using the SPSS Statistics 21 software (IBM).

FCV. Mice were killed by cervical dislocation and decapitated. Coronal slices (300 μm) containing the region of interest (striatum, BNST, or SNr) were prepared as described previously (15, 25) in ice-cold Hepes-buffered artificial cerebrospinal fluid (aCSF) saturated with 95% O_2/5% CO_2. Slices were then maintained in a bicarbonate-buffered aCSF at room temperature before recording. Extracellular dopamine, NE, or 5-HT concentration ($[dopamine]_o$, $[NE]_o$, or $[5\text{-}HT]_o$) were monitored using FCV with 7-μm-diameter carbon fiber microelectrodes (tip length 50–100 μm) and a Millar Voltammeter (Julian Millar, Barts and the London School of Medicine and Dentistry, London, UK) as described previously (15, 26, 27). In brief, the scanning voltage was a triangular waveform (–0.7 V to +1.3 V range vs. Ag/AgCl) at a scan rate of 800 V/s and frequency of 8 Hz. Electrodes were calibrated in 0.5–2 μM 5-HT, dopamine, or NE in experimental media. All data are expressed as means ± SEM, and the sample size, *n*, is the number of observations. The number of animals in each FCV dataset was ≥3. Comparisons for differences in means were assessed by two-way ANOVA and post hoc Bonferroni *t* test or unpaired *t* test using GraphPad Prism 4.0 (GraphPad Software).

HPLC with Electrochemical Detection. Dopamine content was measured by HPLC with electrochemical detection as described previously (16, 20). Following FCV recordings, tissue punches from the dorsal (2 mm in diameter) and ventral striatum (1.2 mm in diameter) from two brain slices per animal were taken and analyzed for dopamine content by HPLC.

Electron Microscopy. Ultrastructural analyses were performed on 3-mo-old mice. Three *SNCA-OVX* and three littermate $Snca^{-/-}$ animals were anesthetized and perfuse-fixed with 0.1% glutaraldehyde and 4% PFA (vol/vol) in 0.1 M phosphate buffer. Sagittal vibratome sections (60 μm) were incubated with primary antibody against TH to identify dopamine neurons, followed by a gold-conjugated secondary antibody and silver-intensification of the gold particles (see ref. 28). Sections were subsequently postfixed in 1% osmium tetroxide and mounted on slides in an electron microscopic resin. Samples of dorsolateral striatum were identified, cut from the sections, and reembedded onto resin blocks and serial ultrathin sections (50–70 nm) were collected and stained with lead citrate. For each animal, 50 images of TH-immunoreactive structures were acquired in a systematically randomized manner (150 images per genotype). In addition, TH-immunoreactive structures forming synaptic specializations were randomly acquired (*SNCA-OVX* = 33; $Snca^{-/-}$ = 29). Digital images of TH-immunoreactive structures and synapses were analyzed using ImageJ and ImageJ plugins PointDensity and PointDensitySyn (16, 29) to measure terminal size, length of synaptic active zone, vesicle number, and distribution. At all stages of tissue processing and ultrastructural analysis the investigators were blinded to animal genotype. Statistical tests were performed using SPSS/PASW Statistics (SPSS) and Matlab (Mathworks).

In Vivo Electrophysiological Recording and Juxtacellular Labeling of Single Neurons. Experiments were performed in urethane-anesthetized (1.5 g/kg, i.p.) 3- to 4-mo-old mice (five $Snca^{-/-}$ and six *SNCA*-OVX) and 18- to 22-mo-old mice (five $Snca^{-/-}$ and six *SNCA*-OVX). Extracellular recordings of single-unit activity in the SNc were made using glass electrodes (10–25 MΩ in situ; tip diameter ~1.5 μm) containing 0.5 M NaCl solution and Neurobiotin (1.5% wt/vol; Vector Laboratories). An electrocorticogram was also recorded above the frontal cortex (18). Following electrophysiological characterization, single neurons were juxtacellularly labeled with Neurobiotin for post hoc verification of location and neurochemical identity (18). We focused our analysis on single-unit activity recorded during robust slow-wave activity, as quantitatively defined from the simultaneous electrocorticogram recordings. Firing pattern was defined according to one of three modes (regular, bursty, or irregular), as detailed previously (30, 31) and in *SI Materials and Methods*. Before statistical comparisons, a Shapiro–Wilk test was used to judge whether datasets were normally distributed ($P < 0.05$ to reject). Statistical comparisons were made using Student *t* tests or Welch *t* tests. The prevalence of firing patterns was compared with a Fisher's exact test.

ACKNOWLEDGMENTS. We thank J. Alegre-Abarrategui, R. Deacon, K. Jennings, C. Johnson, and E. Pissadaki for their expertise in experimental techniques. We thank E. Volpi (Cytogenetics Core, Wellcome Trust Centre for Human Genetics, Oxford; Wellcome Trust Core Award, Grant 090532/Z/09/Z) for FISH analysis. We thank the animal care and veterinary support staff at Oxford University Biomedical Services. This work was supported by the Monument Trust Discovery Award from Parkinson's UK, Wellcome Trust Research Career Development Fellowship GR073141MA (to R.W.-M.), Medical Research Council (MRC) UK Awards U138164490 and U138197109 (to J.P.B. and P.J.M., respectively), and Wellcome Trust Neuroscience Studentship in Neuroscience GR072324MA (to S.L.S.). M.J.D. holds a Girdlers' New Zealand Health Research Council Fellowship; S.J., D.P., and S.A. hold MRC studentships; P.K. is supported by the Clarendon Fund; and D.M.B. holds a Wellcome Trust Senior Research Fellowship.

1. Chesselet M-F, Richter F (2011) Modelling of Parkinson's disease in mice. *Lancet Neurol* 10(12):1108–1118.
2. Polymeropoulos MH, et al. (1997) Mutation in the alpha-synuclein gene identified in families with Parkinson's disease. *Science* 276(5321):2045–2047.
3. Krüger R, et al. (1998) Ala30Pro mutation in the gene encoding alpha-synuclein in Parkinson's disease. *Nat Genet* 18(2):106–108.
4. Zarranz JJ, et al. (2004) The new mutation, E46K, of alpha-synuclein causes Parkinson and Lewy body dementia. *Ann Neurol* 55(2):164–173.
5. Chartier-Harlin MC, et al. (2004) Alpha-synuclein locus duplication as a cause of familial Parkinson's disease. *Lancet* 364(9440):1167–1169.
6. Singleton AB, et al. (2003) alpha-Synuclein locus triplication causes Parkinson's disease. *Science* 302(5646):841.
7. Satake W, et al. (2009) Genome-wide association study identifies common variants at four loci as genetic risk factors for Parkinson's disease. *Nat Genet* 41(12):1303–1307.
8. Simón-Sánchez J, et al. (2009) Genome-wide association study reveals genetic risk underlying Parkinson's disease. *Nat Genet* 41(12):1308–1312.
9. Venda LL, Cragg SJ, Buchman VL, Wade-Martins R (2010) α-Synuclein and dopamine at the crossroads of Parkinson's disease. *Trends Neurosci* 33(12):559–568.
10. Miller DW, et al. (2004) Alpha-synuclein in blood and brain from familial Parkinson disease with SNCA locus triplication. *Neurology* 62(10):1835–1838.
11. Abeliovich A, et al. (2000) Mice lacking alpha-synuclein display functional deficits in the nigrostriatal dopamine system. *Neuron* 25(1):239–252.
12. Neumann M, et al. (2002) Misfolded proteinase K-resistant hyperphosphorylated alpha-synuclein in aged transgenic mice with locomotor deterioration and in human alpha-synucleinopathies. *J Clin Invest* 110(10):1429–1439.
13. Robertson DC, et al. (2004) Developmental loss and resistance to MPTP toxicity of dopaminergic neurones in substantia nigra pars compacta of gamma-synuclein, alpha-synuclein and double alpha/gamma-synuclein null mutant mice. *J Neurochem* 89(5):1126–1136.
14. Al-Wandi A, et al. (2010) Absence of alpha-synuclein affects dopamine metabolism and synaptic markers in the striatum of aging mice. *Neurobiol Aging* 31(5):796–804.
15. Threlfell S, et al. (2012) Striatal dopamine release is triggered by synchronized activity in cholinergic interneurons. *Neuron* 75(1):58–64.
16. Anwar S, et al. (2011) Functional alterations to the nigrostriatal system in mice lacking all three members of the synuclein family. *J Neurosci* 31(20):7264–7274.
17. Nemani VM, et al. (2010) Increased expression of alpha-synuclein reduces neurotransmitter release by inhibiting synaptic vesicle reclustering after endocytosis. *Neuron* 65(1):66–79.
18. Brown MT, Henny P, Bolam JP, Magill PJ (2009) Activity of neurochemically heterogeneous dopaminergic neurons in the substantia nigra during spontaneous and driven changes in brain state. *J Neurosci* 29(9):2915–2925.
19. Gründemann J, Schlaudraff F, Haeckel O, Liss B (2008) Elevated alpha-synuclein mRNA levels in individual UV-laser-microdissected dopaminergic substantia nigra neurons in idiopathic Parkinson's disease. *Nucleic Acids Res* 36(7):e38.
20. Senior SL, et al. (2008) Increased striatal dopamine release and hyperdopaminergic-like behaviour in mice lacking both alpha-synuclein and gamma-synuclein. *Eur J Neurosci* 27(4):947–957.
21. Smith Y, Kieval JZ (2000) Anatomy of the dopamine system in the basal ganglia. *Trends Neurosci* 23(10, Suppl):S28–S33.
22. Sun A, Nguyen XV, Bing G (2002) Comparative analysis of an improved thioflavin-s stain, Gallyas silver stain, and immunohistochemistry for neurofibrillary tangle demonstration on the same sections. *J Histochem Cytochem* 50(4):463–472.
23. Franklin KBJ, Paxinos G (2007) *The Mouse Brain in Stereotaxic Coordinates* (Academic, New York), 3rd Ed.
24. Taylor TN, et al. (2009) Nonmotor symptoms of Parkinson's disease revealed in an animal model with reduced monoamine storage capacity. *J Neurosci* 29(25):8103–8113.
25. Threlfell S, et al. (2010) Striatal muscarinic receptors promote activity dependence of dopamine transmission via distinct receptor subtypes on cholinergic interneurons in ventral versus dorsal striatum. *J Neurosci* 30(9):3398–3408.
26. Jennings KA, Lesch KP, Sharp T, Cragg SJ (2010) Non-linear relationship between 5-HT transporter gene expression and frequency sensitivity of 5-HT signals. *J Neurochem* 115(4):965–973.
27. Threlfell S, et al. (2004) Histamine H3 receptors inhibit serotonin release in substantia nigra pars reticulata. *J Neurosci* 24(40):8704–8710.
28. Moss J, Bolam JP (2008) A dopaminergic axon lattice in the striatum and its relationship with cortical and thalamic terminals. *J Neurosci* 28(44):11221–11230.
29. Larsson M, Broman J (2005) Different basal levels of CaMKII phosphorylated at Thr286/287 at nociceptive and low-threshold primary afferent synapses. *Eur J Neurosci* 21(9):2445–2458.
30. Tepper JM, Martin LP, Anderson DR (1995) GABAA receptor-mediated inhibition of rat substantia nigra dopaminergic neurons by pars reticulata projection neurons. *J Neurosci* 15(4):3092–3103.
31. Paladini CA, Tepper JM (1999) GABA(A) and GABA(B) antagonists differentially affect the firing pattern of substantia nigra dopaminergic neurons in vivo. *Synapse* 32(3):165–176.